# Atomistic stress analysis of an MMA thin film on an Au (111) substrate

# MMA 薄膜於金(111)基板上之原子級應力分析

Ming-Liang Liao<sup>1</sup>, Fu-Yen Jian<sup>1</sup>, Shin-Pon Ju<sup>2</sup>, Wen-Jay Lee<sup>2</sup>, Ching-Ho Cheng<sup>2</sup> 廖明亮<sup>1</sup> 簡富彦<sup>1</sup> 朱訓鵬<sup>2</sup> 李玟頡<sup>2</sup> 鄭敬禾<sup>2</sup>

<sup>1</sup> Department of Aircraft Engineering, Air Force Institute of Technology, Kaohsiung, Taiwan, R.O.C.

<sup>2</sup> Department of Mechanical and Electro-Mechanical Engineering, National Sun Yat-Sen University, Kaohsiung, Taiwan, R.O.C.

1空軍航空技術學院飛機工程學系

2國立中山大學機械與機電工程學系

#### Abstract

Atomistic stress analysis in a methyl methacrylate (MMA) thin film on an Au (111) substrate is performed by the molecular dynamics simulations. Distributions of the normal stress, the tangential stress, and the surface tension across the film thickness are all examined in the present study. To inspect the stresses across the thickness of the MMA thin film, the whole thickness are divided into contact, transition, bulk, and surface regions according to the free energy profile of the MMA thin film. It is observed that in the contact region there is an obvious peak in the density profile of the MMA molecules. Temperature effects on the density profile are significant in this region and the density of the MMA molecules obviously decreases with an increase in the system temperature. The free energy in the bulk region is near zero and grows progressively in the surface region. In the area near the Au (111) surface, on average, the normal stress of the thin film is in compression and the surface tension is positive. In the bulk region, the normal stress and surface tension behave a fluctuation about a free stress state. In the surface region, however, the normal stress exhibits a tension state and it yields a negative surface tension. The tangential stress is lower than the normal stress and thus has lesser contribution to the surface tension in the current investigation. It is also noticed that the temperature effects on the stress and surface tension distributions are not manifest in the present study.

**Keywords:** number density, free energy, normal stress, tangential stress, surface tension, molecular dynamics simulations

# 摘要

本文以分子動力學模擬的方法來執行甲基丙烯酸甲酯(MMA)薄膜於金(111)基板上之原子級應力分析。文中分別探討沿 MMA 薄膜厚度方向之正向應力、切向應力與表面張力之分布。為了便於檢視 MMA 薄膜之原子級應力,文中依據 MMA 薄膜之自由能分布,將薄膜沿厚度方向區分為接觸區、過渡區、塊材區與表面區等四個區域。由本文之模擬結果可知,於接觸區內 MMA 分子之數密度分布呈現明顯之峰值,而且此區域內 MMA 分子之密度分布受溫度之影響亦較顯著,隨著電的升高,其數密度有明顯降低的趨勢。此外薄膜於塊材區內之自由能趨近於零而於表面區內其自由能則有明顯的增加。在應力方面,於接近金(111)基板表面之。成,平均而言薄膜之正向應力為壓應力,而有正的表面張力。在塊材區內,薄膜之正向應力與表面張力皆呈現出於零值附近震盪之狀態。然而在表面區內,薄膜之正向應力為張應力,而其表面張力為負值。由模擬之結果亦可知,由於薄膜之正向應力為張應力,而其表面張力為負值。由模擬之結果亦可知,由於薄膜之正向應力為張應力,而其表面張力為負值。由模擬之結果亦可知,由於薄膜之正向應力為張應力,而其表面張力為負值。由模擬之結果亦可知,由於薄膜之正

關鍵字: 數密度、自由能、正向應力、切向應力、表面張力、分子動力學模擬

## 1. Introduction

The structural and dynamic behavior of polymer molecules in a thin film on a solid substrate has attracted considerable interest in recent years [1-4]. This interest arises primarily because such molecules exhibit different material properties than those in the bulk and have the potential for application in such diverse fields as nanoimprinting [5], nanolithography [5, 6], nano-electronic devices and storage chips. One of the most exciting applications of very thin films is that of a new form of atomic force microscope (AFM)-based data storage medium known as "Millipede", in which a thin (50 nm) PMMA layer is used as an indentation substrate on the storage substrate [7-9]. This novel technique provides an ultrahigh storage density (about 400-500 Gb/in<sup>2</sup>) [7] and has many remarkable features such as a terabit capacity, a small form factor and a high data rate.

Many empirical studies have been conducted to investigate the surface and thickness effects of polymer thin films on a solid substrate. In recent studies, Keddie [10, 11] found that for polystyrene (PS) films, the film thickness has a significant effect on the glass transition temperature,  $T_g$ , when the film has a thickness of less than 40 nm. However, for poly (methyl methacrylate) (PMMA) thin films,  $T_g$  is relatively insensitive to the film thickness, but is significantly influenced by the substrate material. For example, van Melick et al. [12] showed that the value of  $T_g$  reduced when the PMMA film was deposited on an Au (111) surface, but increased when the film was grown on a silicon substrate with a native oxide layer. In recent studies, various experimental approaches have been employed to observe the structure and dynamic properties of polymer thin films on solid surfaces, including thermal probe measurements [13, 14], ellipsometry [10], positron

annihilation lifetime spectroscopy [15], Xreflectivity [16] and dielectric relaxation [17-20]. However, it is difficult to observe the structural arrangement of the polymer molecules at the interface between the thin film and the substrate at the atomic level using direct experimental methods. Accordingly, experimental approaches fail to provide an adequate understanding of the influence of the interface on the structure and properties of the thin film. However, the interface effect becomes increasingly important when the thickness of the film is less than several nanometers since the thickness of the interface then accounts for a considerable fraction of the total film thickness. Molecular dynamics (MD) simulations overcome the limitations of traditional empirical approaches and enable detailed observations of the interfacial behavior between a thin polymer film and a solid substrate at the atomic scale [21-24]. Xia conducted MDsimulations investigate the variation in density profile of n-hexadecane films with different thicknesses on Au (111) surfaces. The results showed that the density profile had an oscillatory behavior in the region of the thin film near the interface, but gradually became smooth at a greater distance from the substrate. Daoulas [22] explored the volumetric, structural and conformational aspects of PE melt/graphite and PE melt/vacuum interfaces, respectively. The corresponding density profiles indicated that the PE thin film had at least three adsorption layers near the substrate. The chain conformations were mainly flattened in the first adsorption layer, but the polymer molecules gradually tended

toward their bulk characteristics at greater distances from the solid surface. Additionally, sudden changes in the dihedral angle distribution of molecules were observed between one absorption layer and the next. The topics of liquids adsorbed on solid surfaces have been widely research using simulation approaches [25-31]. For example, Xin et al. [27] studied the spreading of polymer droplets of functional and non-functional **PFPE** (Perfluoropolyether) on solid surfaces using the coarse-grained MD simulations. The results revealed that the non-functional PFPE films will form caplike structures on the substrate, and the functional PFPE film will give rise to a hat structure in the spreading process. Grest et al. [28] conducted MD simulations to examine the spreading of liquid polymer droplets of varying chain lengths on The chemically patterned surfaces. results numerical showed that the spreading behavior was governed by the pattern width, the length of the polymer chain and the interaction strength of the lyophilic strips.

From the discussions above, it is clear that MD simulation provides a powerful for investigating the interfacial behavior of polymer thin films on solid substrates at the atomic level. Accordingly, the present study adopts the MD simulation approach to investigate the molecular adsorption mechanism of methyl methacrylate (MMA) thin films on an Au (111) substrate. The density and free energy profiles were calculated to examine the arrangement characteristics of the MMA thin film. Temperature effects on the characteristics arrangement were

discussed. The atomistic stresses and the surface tension across the thickness of the MMA thin film were then investigated and the temperature effects on the stresses were thus examined. Finally, we discussed and summarized the important finding of the present research.

### 2. Simulation model

The MD simulation model used in the present research consists of an MMAoligomer thin film and an Au substrate on which the MMA oligomers are deposited. Fig. 1 depicts a schematic diagram of the present simulation model. There are three different groups of interactions existing in the simulation model, including 1) the intra- and intermolecular interactions of MMA oligomers; 2) the interaction of Au atoms; 3) the interaction between the MMA oligomers and the Au atoms. In the current MD simulations, three different potentials were employed to model the three groups of interactions. First, the **ENCAD** (Energy Calculations Dynamics) potential [32, 33] was chosen to model the atomic interaction between the intra- and intermolecular interactions of the MMA oligomers. The interaction between the Au atoms of the substrate was described by the tight-binding potential [34, 35], whereas the Dreiding force field [36] was used to model the interaction between the MMA oligomers and the Au atoms. The expressions for the three potentials are described below.

## 2.1. Potential for MMA oligomers

In the present research, the ENCAD (Energy Calculations and Dynamics) potential [32] was employed to model the atomic interaction between the MMA

molecules and the intra-interaction of a MMA molecule. In this model, the potential force field (FF) is expressed as the sum of the bond stretching energy  $U_{\rm bond}$ , the bond bending energy  $U_{\rm bend}$ , the bond torsion energy  $U_{\rm torsion}$ , the van der Waals energy  $U_{\rm vdw}$ , and the electrostatic energy  $U_{\rm els}$ . Accordingly, the total potential,  $U_{\rm vdw}$ , is given by:

 $U = U_{\text{bond}} + U_{\text{bend}} + U_{\text{torsion}} + U_{\text{vdw}} + U_{\text{els}}$ (1) with

$$Ubond = \sum_{i} K_b^{i} (b_i - b_0)^2$$
 (2)

$$Ubend = \sum_{i} K_{\theta}^{i} (\theta_{i} - \theta_{0})^{2}$$
 (3)

$$Utorsion = \sum_{i} K_{\varphi}^{i} \left\{ 1 - \cos \left[ n^{i} (\varphi_{i} - \varphi_{0}^{i}) \right] \right\}$$
 (4)

$$Uvdw =$$

$$\sum_{i,j} \left[ A_{sc} \varepsilon^{ij} (r_0^{ij} / r_{ij})^{12} - 2\varepsilon^{ij} (r_0^{ij} / r_{ij})^6 - S_{vdw}(r_{ij}) \right] (5)$$

$$Uels = 332 \sum_{i,j} \left[ q^{i} q^{j} / r_{ij} - S_{els}(r_{ij}) \right]$$
 (6)

where  $K_b^i$ ,  $K_\theta^i$  and  $K_\omega^i$  are force constants representing the bond stretching, bond bending and torsion barrier of the ith bond, respectively, and  $b_i$ ,  $\theta_i$ ,  $\varphi_i$ ,  $b_0$ ,  $\theta_0$  and  $\varphi_0$ are the ith bond length, the ith bending angle, the ith torsion angle, equilibrium bond length, the equilibrium bending angle and the equilibrium torsion angle, respectively. The bond torsion energy can be represented either by the true dihedral angles or the out-of-plane dihedral angles, and is represented by a cosine function with a periodicity  $n^i$  and an equilibrium torsion angle  $\varphi_0$ . All the summations in the bonded energy terms (Equations 2 to 4) are carried out over all corresponding bonds.

The van der Waals energy is expressed using the Lennard-Jones 6-12 potential, which includes both repulsive attractive terms. In this potential model,  $r_{ij}$ indicates the atomic distance between atoms i and j in a non-bonded pair, and  $A_{sc}$ is used to compensate for the interaction lost at small cutoff distances. The value of  $A_{sc}$  is determined by the cutoff distance specified in the ENCAD model. In the present simulations, the cutoff distance was specified as 8 Å and the value of  $A_{sc}$ was assumed to be 0.84. These values were chosen because they were commonly utilized in the studies of MMA thin films. The values of the energy parameter,  $\varepsilon^{ij}$ , the distance parameter,  $r_0^{ij}$ , and the truncation shift function,  $S_{vdw}$ , for the van der Waals potential can be found from Levitt et al. [32, 33]. The electrostatic energy in the ENCAD potential force field is modeled using the Coulomb potential, in which  $q^i$  and  $q^j$  (in units of electrons) represent the partial charges of atoms i and j of the MAA molecules within the cutoff distance and the truncation shift function,  $S_{els}$ , can be obtained from the reference [32, 33]. The constant 332 in Equation 6 is employed to convert the energy  $U_{\rm els}$  to that with a unit of kcal/mol. The summations of the non-bonded terms ( $U_{\rm vdw}$  and  $U_{\rm els}$ ) are executed over all non-bonded atom pairs i and j closer than the cutoff distance. Moreover, the potential parameters in the ENCAD force field are derived from abinitio quantum mechanics, spectroscopy and crystallography. For the present study, these parameters were taken from those of Levitt et al. [32, 33]. These parameter values were determined to reproduce energetic, structural, and dynamic properties found from ab initio quantum mechanics calculations, spectroscopic measurements, and crystallographic data.

## 2.2. Potential for Au atoms

The interatomic force between the Au atoms in the substrate was modeled using the tight-binding potential [34, 35]. The main difference between a many-body potential model and a pairwise potential model is that the former considers the interaction between any two atoms to depend not only on the two atoms themselves, but also upon the surrounding atoms. It has been shown that the tightbinding potential yields more accurate predictions of some characteristics of certain transition metals than the EAM (Embedded Atom Method) approach [34, 35]. Moreover, the algorithm for computing this potential is simpler than that required for EAM. The tight-binding potential model commences by summing the band energy, which is characterized by the second moment of the d-band density of state, and a pairwise potential energy of the Born-Mayer type. The interatomic energy of atom i is thus expressed as:

$$U^i = U_R^i + U_B^i \tag{7}$$

with repulsive energy and bonding energy have the following forms

$$U_R^i = \sum_{i} A \cdot \exp\left\{-p\left(r_{ij} / r_0 - 1\right)\right\}$$
(8)

$$U_B^i = -\left\{ \sum_{j} \xi^2 \cdot \exp\left[-2q\left(r_{ij}/r_0 - 1\right)\right] \right\}^{1/2}$$
 (9)

where  $\xi$  is an effective hopping integral,  $r_{ij}$  is the distance between atoms i and j,

and  $r_0$  is the first-neighbor distance. The parameters A, p, q, and  $\xi$  are determined by incorporating the experimental data relating to the cohesive energy, the lattice parameter, the bulk modulus and the shear elastic constants  $C_{44}$  and  $C = (C_{11}-C_{12})/2$ , respectively. The parameter values of the tight-binding potential model employed in the present simulations are taken from the reference [35] and are 0.2061 eV, 1.790 eV, 10.229, and 4.036 for A,  $\xi$ , p, and q, respectively. These parameter values were determined using experimental data related to the cohesive energy, lattice parameters, bulk modulus, and shear elastic constants.

# 2.3. Potential for interaction between MMA oligomers and Au atoms

The interaction between the Au substrate and the adsorbed MMA molecules is described using the Dreiding force field [36], which has the following exponential-6 form:

$$U_{ij} = D \left[ \left( \frac{6}{z - 6} \right) \exp \left( \varsigma \left( 1 - \frac{r_{ij}}{r} \right) \right) - \left( \frac{\varsigma}{\varsigma - 6} \right) \left( \frac{r_{ij}}{r} \right)^{-6} \right] (10)$$

where D is the energy barrier, r is the distance between the gold atom and the atom in the MMA molecule in an energy minimum state,  $r_{ij}$  is the distance between the gold atom and the atom in the MMA molecule, and  $\varsigma$  is a dimensionless constant whose value is dependent on the curvature or stiffness of the inner repulsive wall. The values of these parameters D, r, and  $\varsigma$  are taken from the reference [36] and are listed in Table 1. These parameter values were optimized by fitting the geometry and binding energy calculated from quantum mechanics for organic molecules on Au (111) surfaces [36]. In addition, the parameter values were verified by experimental data as illustrated in the results of the reference, where structures and interfacial properties of self-assembled monolayers on Au (111) surfaces were examined. Our previous research also demonstrated that the parameter values applied very well to the investigation of structures and properties of MMA thin films on an Au (111) substrate.

#### 2.4. Simulation details

The simulation system consists of an MMA thin film with 378 MMA molecules, which have a molecular formula of CH<sub>2</sub>=C(CH<sub>3</sub>)COOCH<sub>3</sub>, deposited on an Au (111) substrate with a thickness of 14 Å and comprising six separate Au layers. The simulation box has dimensions of  $L_x$ = 54.95 Å and  $L_y$ = 49.03 Å and periodic boundary conditions are imposed in both the x- and the y-directions. A virtual repulsive wall is introduced at an initial height of 81 Å above the bottom of the substrate. The objective of this wall was to confine the MMA molecules above the Au surface. Adopting a similar approach to that employed by Jang et al. [36], the following four-step procedure performed to obtain the equilibrium structure of the MAA molecules on the Au (111) surface: (1) The MAA molecules were positioned on the Au (111) surface with an initial density of 0.35 g/cm<sup>3</sup> and were then gradually compressed to a density of 0.94 g/cm<sup>3</sup> (consistent with the experimental value) by moving the wall toward the substrate repulsive surface. To prevent the configuration from becoming trapped at a local minimum energy, the system was maintained at a temperature of 500 K for 500 ps. (2) Once

the required density had been obtained, the system was annealed from 500 K to room temperature at a cooling rate of 3 K/ps. The system was then equilibrated at room temperature for 100 ps. (3) The repulsive wall was gradually removed at room temperature. Subsequently, the temperature was gradually increased to 400 K. This process was use to release the MMA thin film, and reduce the artificial effect of the virtual repulsive wall. (4) Finally, an annealing process was performed to reduce the temperature from 400 K to the target temperature, and then the system was equilibrated at this target temperature for another 40 ps. In the simulations, the velocities of the atoms were randomly assigned according to Maxwell distribution, and the velocity-rescaling thermostat [37, 38] was employed to maintain a uniform temperature. The time integration of the Newtonian equations of motion was performed using the Verlet algorithm to obtain the new velocities and positions of each atom [37, 38]. Moreover, a canonical (NVT) ensemble was employed during the simulations and data in the final 10 ps were collected and averaged to examine simulation results.

A canonical (NVT) ensemble was utilized in the present simulations because it can provide an easier way to calculate density distributions of the MMA thin films. To justify the use of a canonical ensemble in computing and comparing density distributions of the various cases studied in the current research, the pressure variations among the cases were examined. Since the external forces applied on the simulation system are negligible, the pressure variations among

various cases of the present study are not apparent. This implies that the external forces imposed by the boundaries in both the x- and y-directions can be neglected. Because no external loads were applied on the top surface of the MMA thin film, the system under simulation can be regarded as an unloaded system. By the same reasoning, the present system can also be regarded as unloaded. Therefore, pressure among various cases of the current study would be fairly close and it would not yield problems when a canonical (NVT) ensemble was utilized in calculating and comparing the density distributions of the MMA-oligomer thin films.

Figure presents schematic 1 a illustration of the relaxed MMA film on the Au (111) substrate. As shown, the substrate was modeled as six separate layers, with five layers providing a thermal control function and the lowest layer used to fix the simulation system. The goal of the current MD simulations was to investigate the atomistic stresses and the surface tension across the thickness of the MMA thin film and the temperature effects on the stresses. For the study of the temperature effects, a temperature range from 200 to 300 K was selected. The MD simulations were performed computer code developed by the authors.

# 3. Results and discussion

Figure 2 shows variations of number density and free energy (or equivalently the potential of mean force, PMF) across thickness of the MMA thin film at temperatures of 200, 245 and 300 K. The number density is computed by counting the number of molecules in a slab of

thickness 0.6 Å positioned parallel to the Au (111) surface at various heights above the substrate. Meanwhile, the value of the local free energy is derived as [39]:

$$G(z) = -k_B T \ln[\rho(z)/\rho_{bulk}]$$
(11)

where  $k_B$ , T,  $\rho(z)$ , and  $\rho_{bulk}$  are the Boltzmann constant, the system temperature, the local number density at height z and the bulk number density, respectively. The density variations at 200, 245, and 300 K are shown in the upper panel of Figure 2. It is observed that the density profile at each temperature has a prominent peak at the interface of the MMA thin film and the Au (111) substrate. However, the number density reduces significantly within a short distance of the interface before increasing once again. Thereafter, the density fluctuates about an constant approximately value reducing to zero at the surface of the thin film. According to the PMF profiles shown in the lower panel of Figure 2, the density distribution in the z-direction can be divided into four distinct regions, namely the contact region (I), the transition region (II), the bulk region (III) and the surface region (IV).

In the contact region (region I), it is noted that the value of PMF has a negative value, which results in a higher number density and also indicates that the Au (111) surface and the MMA molecules have the attractive interaction. In the bulk region (region III), the PMF profiles have an average value of zero and fluctuate only mildly. The number density in the bulk region also has an approximately constant value. As expected, this indicates that the bulk region of the thin film behaves like

the bulk MMA material. The contact region and the bulk region are separated by a transition region (region II), within which the density reduces from the high density of the contact region to the low density of the bulk region. The interaction between the substrate and the MMA molecules has a significant effect on the structure of the MMA thin film only in the contact region. Consequently, the compact stacking of the MMA molecules in the contact region prevents other MMA molecules from having a density as high as in the bulk region. This leads the transition region to have a density lower than that in the bulk region and to have positive free energy. In the surface region (region IV), the density distributions drop gradually to zero but the free energy distributions grow progressively. This means that the MMA molecules in the surface region have much lower stability than those in the other regions. In regard to the temperature effects, it is observed that the average density of the MMA film reduces with an increase in the temperature, especially in the contact region.

The atomistic stresses of the MMA thin films examined in the present study are the normal stress and the tangential stress. The stresses can be calculated from the pressure tensor of the Kirkwood-Buff theory [40] with

$$P_N(z) = \rho(z)k_B T - \frac{1}{V_{slab}} \left\langle \sum_{i,j} \frac{z_{ij}^2}{r_{ij}} \frac{dU(r_{ij})}{dr_{ij}} \right\rangle$$
(12)

$$P_T(z) = \rho(z)k_BT - \frac{1}{V_{slab}} \left\langle \sum_{i,j} \frac{x_{ij}^2 + y_{ij}^2}{2r_{ij}} \frac{dU(r_{ij})}{dr_{ij}} \right\rangle (13)$$

where  $P_N(z)$  and  $P_T(z)$  are respectively the normal and the tangential components of

the pressure tensor (i. e. the normal and tangential stresses) in a slab in the zdirection,  $\rho(z)$  denotes the number density of a slab positioned at point z on the zaxis,  $V_{slab}$  is the volume of the slab,  $k_B$ , is the Boltzmann constant, and T is the system temperature. The contents of the large angle brackets represent ensemble average of all the atoms located in the slab. The quantity  $r_{ij}$  is the distance between atoms i and j, whereas  $x_{ij}$ ,  $y_{ij}$  and  $z_{ij}$  are the three components of the vector from atom i to atom j, respectively, and  $U(r_{ii})$  is the potential energy of the atomic pair i and j. The Kirkwood-Buff theory has been used successfully in former studies of interfaces complicated mediated surfactant molecules [39] and of general liquid/vapor interfaces [41-43].

Figure 3 presents variations of the normal stress across thickness of the MMA thin film at the various system temperatures. According to the Kirkwood-Buff theory, a positive stress indicates a compressive stress of the analyzed volume. It is observed that at each of the temperatures considered, the normal stress of the thin film, on average, is in compression near the Au (111) surface. result is consistent with presented in Figure 2, which shows a compact stacking of MMA molecules (i.e. a higher density) near the Au (111) surface and thus there exists a compressive normal stress. The normal stress in the bulk region, however, exhibits a fluctuation about a zero state (i.e. a free stress state). This is also coherent to the fluctuation in the density profile of the bulk region depicted in Figure 2 and corresponds to the behavior of the bulk MMA material.

Moreover, the normal stress in the surface region is in tension at the various system temperatures. The through thickness distribution of the normal stress of the current study are similar to that of Jang *et al.* [36], although thin films from a different material were examined there.

Figure 4 displays variations of the tangential stress across thickness of the MMA thin film at the various It is noticed temperatures. that the tangential stress is lower than the normal stress and behaves a fluctuation about a zero state through the film thickness for the system temperatures. Similar to the situation for the normal stress, temperature effects on the tangential stress distribution are not apparent.

Figure 5 shows variations of the surface tension across thickness of the MMA film at various system temperatures. The surface tension can be calculated from difference of the normal and tangential stresses [36]:

$$\gamma = \int_{L_1}^{L_2} [P_N(z) - P_T(z)] dz$$
 (14)

where  $L_1$  and  $L_2$  indicate the limits of the integration range, i.e. the z coordinates representing the slab thickness in the current case. From Figure 5, it is observed that the surface tension of the thin film, on average, is positive near the Au (111) surface. This is because the MMA molecules in this area are adsorbed on the Au (111) surface and have a compact stacking. Thus yields a positive surface tension in this area. In the bulk region the surface tension also behaves a fluctuation about a zero state whereas has a negative value in the surface region. The negative

surface tension is ascribed to the tensile normal stress in the surface region (as discussed in Figure 3). The similar tendency between the through thickness distributions of the surface tension and the normal stress is owing to the lesser contribution from the tangential stress to the surface tension in the present cases (cf. Figures 3 and 4).

#### 4. Conclusions

Atomistic stress analysis of a MMA thin film on an Au (111) substrate has been performed by the molecular dynamics simulations. For ease of investigation, the whole thickness is divided into contact, transition, bulk, and surface regions according to the free energy profile of the MMA thin film. It is observed that in the contact region there is an obvious peak in the density profile of the MMA molecules, which means that the MMA molecules have a higher concentration (i.e. a compact stacking) in the contact Temperature effects on the density profile are significant in the contact region. As the temperature increases, the density of the MMA molecules obviously decreases in this region. The free energy in the bulk region near zero and grows progressively in the surface region. This means that the MMA molecules in the surface region have much lower stability than those in the other regions.

The normal stress of the thin film, on average, is in compression near the Au (111) surface. However, it behaves a fluctuation about a free stress state in the bulk region and exhibits a tension state in the surface region. The tangential stress is lower than the normal stress and thus has

smaller contribution to the surface tension in the present cases. Furthermore, the surface tension of the thin film, on average, is positive near the Au (111) surface. In the bulk region the surface tension also behaves a fluctuation about a zero state whereas has a negative value in the surface region. It is also observed that the temperature effects on the stress and surface tension distributions are not significant in the current study.

It should be noted that an Au (111) substrate was selected in the present study because the (111) crystal plane of gold is a highly symmetric crystal and has a maximum planar atom density, which lets have many applications The conformational nanotechnology. behavior of MMA-oligomer thin films on a gold substrate with a different orientation, e.g. (100) or (110), might differ from that of the present case. This is an interesting issue worthy of further investigation. Nevertheless, some aspects could be inferred based on results from related studies. In our earlier research on the behavior of water molecules confined between parallel gold plates [44], we found that the molecules on the Au (110) surface had behavior distinct from that on the Au (111) and (100) surfaces. The distinction between the behavior of water molecules on the Au (111) and (100) surfaces was not evident. Similar findings were obtained for metal oxide thin films [45, 46] and polymer thin films [47] on Au (111), (100), and (110) substrates. Thus, one could anticipate that the MMA-oligomer thin film on an Au (100) substrate would have conformational behavior similar to that on an Au (111) substrate. However,

due to the loose structure and low symmetry of the (110) crystal plane, the MMA-oligomer thin film on an Au (110) substrate might have different conformational behavior. Detailed comparisons require further analysis.

### 5. References

- J. R. Dutcher, K. Dalnoki-Veress, J.A. Forrest, Supermolecular Structure in Confined Geometries, ACS Symposium Series (American Chemical Society), 1999.
- 2. J. A. Forrest, R.A.L. Jones, *Polymer Surfaces, Interfaces and Thin Films*, World Scientific, Singapore, 2000.
- 3. B. Frick, R. Zorn, H. Büttner, Proceedings of the International Workshop on Dynamics in Confinement, EDP Sciences, 2000.
- J.A. Forrest, K. Dalnoki-Veress, "The glass transition in thin polymer films,"
   *Adv. Colloid Interface Sci.*, vol. 94, pp. 167, 2001.
- S. Zankovych, T. Hoffmann, J. Seekamp, J. U. Bruch, and C. M. Torres, "Nanoimprint lithography: challenges and prospects," *Nanotechnology*, vol. 12, pp. 91, 2001.
- C. Martín, G. Rius, X. Borrisé, and F. Pérez-Murano, "Nanolithography on thin layers of PMMA using atomic force microscopy," *Nanotechnology*, vol. 16, pp. 1016, 2005.
- 7. P. Vettiger, M. Despont, U. Drechsler, U. Dürig, W. Häberle, M. I. Lutwyche, H. E. Rothuizen, R. Stutz, R. Widmer, and G. K. Binnig, "The 'Millipede'-more than one thousand tips for future AFM data storage," *IBM J. Res. Develop.*, vol. 44, pp. 323, 2000.

- 8. P. Vettiger, J. Brugger, M. Despont, U. Drechsler, U. Dürig, W. Häberle, M. I. Lutwyche, H. E. Rothuizen, R. Stutz, R. Widmer, and G. K. Binnig, "Ultrahigh density, high-data-rate NEMS-based AFM data storage system,"

  Microelecronic Engineering, vol. 46, pp. 11, 1999.
- G. Binnig, M. Despont, U. Drechsler, W. Häberle, M. Lutwyche, P. Vettiger, H. J. Mamin, B. W. Chui and T. W. Kenny, "Ultrahigh-density atomic force microscopy data storage with erase capability," *Appl. Phys. Lett.*, vol. 74, pp. 1329, 1999.
- 10. J.L. Keddie, R.A.L. Jones, and R.A. Cory, "Size-dependent depression of the glass transition temperature in polymer films," *Europhys. Lett.*, vol. 27, pp. 59, 1994.
- 11. J.L. Keddie, R.A.L. Jones, and R.A. Cory, "Interface and surface effects on the glass-transition temperature in thin polymer films," *Faraday Discuss. Chem. Soc.*, vol. 98, pp. 219, 1994.
- 12. H. van Melick, A. van Dijken, J. Den Toonder, L. Govaert, and H. Meijer, "Near-surface mechanical properties of amorphous polymers," *Philosophical Magazine A*, vol. 82, pp. 2093, 2002.
- 13. K. Fukao, and Y. Miyamoto, "Glass transitions and dynamics in thin polymer films: Dielectric relaxation of thin films of polystyrene," *Phys. Rev. E*, vol. 61, pp. 1743, 2000.
- 14. C. Bauer, R. Böhmer, S. Moreno-Flores, R. Richert, H. Sillescu, and D. Neher, "Capacitive scanning dilatometry and frequency-dependent thermal expansion of polymer films,"

- Phys. Rev. E, vol. 61, pp. 1755, 2000.
- 15. G. B. de Maggio, W.E. Frieze, D. W. Gidley, M. Zhu, H. A. Hristov, and A. F. Yee, "Interface and surface effects on the glass transition in thin polystyrene films," *Phys. Rev. Lett.*, vol. 78, pp. 1524, 1997.
- 16. W. E. Wallace, J. H. van Zanten, and W. L. Wu, "Influence of an impenetrable interface on a polymer glass-transition temperature," *Phys. Rev. E*, vol. 52, pp. R3329, 1995.
- 17. K. Fukao, and Y. Miyamoto, "Glass transition temperature and dynamics of  $\alpha$ -process in thin polymer films," *Europhys. Lett.*, vol. 46, pp. 649, 1999.
- 18. K. Fukao, and Y. Miyamoto, "Slow dynamics near glass transitions in thin polymer films," *Phys. Rev. E*, vol. 64, pp. 011803, 2001.
- 19. K. Fukao, S. Uno, Y. Miyamoto, A. Hoshino, and H. Miyaji, "Dynamics of α and β processes in thin polymer films: poly(vinyl acetate) and poly(methyl methacrylate)," Phys. Rev. E, vol. 64, pp. 051807, 2001.
- 20. L. Hartmann, Th. Kratzmüller, H.-G. Braun, and F. Kremer, "Molecular dynamics of grafted PBLG in the swollen and in the dried state," *Macromol. Rapid Commun.*, vol. 21, pp. 814, 2000.
- 21. T. K. Xia, J. Ouyang, M. W. Ribarsky, U. Landman, "Interfacial alkane films," *Phys. Rev. Lett.*, vol. 69, pp. 1967, 1992.
- 22. K. C. Daoulas, V. A. Harmandaris, and V. G. Mavrantzas, "Detailed atomistic simulation of a polymer melt/solid interface: structure, density, and conformation of a thin film of

- polyethylene melt adsorbed on graphite," *Macromolecules*, vol. 38, pp. 5780, 2005.
- 23. L. Hartmann, W. Gorbatschow, J. Hauwede, and F. Kremer, "Molecular dynamics in thin films of isotactic poly(methyl methacrylate)," *Eur. Phys. J. E*, vol. 8, pp. 145, 2002.
- 24. H. Dominguez, A. Gama Goicochea, N. Mendoza, J. Alejandre, "Computer simulations of surfactant monolayers at solid walls," *J. Coll. And Inter. Sci.*, vol. 297, pp. 370, 2006.
- S. Matsumoto, S. Maruyama, and H. Saruwatari, ASME/JSME Thermal Engineering Conference, vol. 2, pp. 557, 1995.
- 26. M. H. Adão, M. D. Ruijter, M. Voué, and J. D. Coninck, "Droplet spreading on heterogeneous substrates using molecular dynamics," *Phys. Rev. E*, vol. 59, pp. 746, 1999.
- 27. X. Li, Y. Hu, and H. Wang, "Modeling of lubricant spreading on a solid substrate," J. Appl. Phys., vol. 99, pp. 024905, 2006.
- 28. G. S. Grest, D. R. Heine, and E. B. Webb, "Liquid nanodroplets spreading on chemically patterned surfaces," *Langmuir*, vol. 22, pp. 4745, 2006.
- 29. M. Patra, and P. Linse, "Simulation of grafted polymers on nanopatterned surfaces," *Nano Lett.*, vol. 6, pp. 133, 2005.
- 30. T. Kimura, and S. Maruyama, *The 6th ASME-JSME Thermal Engineering Joint Conference*, March 16, 2003.
- 31. B. Shi, S. Sinha, V. K. Dhir, ASME International Mechanical Engineering Congress and Exposition, Nov. 5, 2005.

- 32. M. Levitt, M. Hirshberg, R. Sharon, and V. Daggett, "Potential energy function and parameters for simulations of the molecular dynamics of proteins and nucleic acids in solution," *Com. Phys. Com*, vol. 91, pp. 215, 1995.
- 33. M. Levitt, M. Hirshberg, R. Sharon, K. E. Laiding, and V. Daggett, "Calibration and testing of a water model for simulation of the molecular dynamics of proteins and nucleic acids in solution," *J. Phys. Chem. B*, vol. 101, pp. 5051, 1997.
- 34. V. Rosato, M. Guillope, and B. Legrand, "Thermodynamical and structural properties of F.C.C. transition metals using a simple tight-binding model," *Phil. Mag. A*, vol. 59, pp. 321, 1989.
- 35. F. Cleri, and V. Rosato, "Tight-binding potentials for transition metals and alloys," *Phys. Rev. B*, vol. 48, pp. 22, 1993.
- 36. S. S. Jang, Y. H. Jang, Y. H. Kim, W. A.Goddard III, A. H. Flood, B. W. Laursen, H. R. Tseng, J. F. Stoddart, J. O. Jeppesen, J. W. Choi, David W., S. Delonno, and J. R. Heath, " Structures and properties of selfassembled monolayers of bistable [2]rotaxanes on Au (111) surfaces from molecular dynamics simulations validated with experiment," J. Am. Chem. Soc., vol. 127, pp. 1563, 2005.
- 37. J. M. Haile, *Molecular Dynamics Simulation*, Wiley Interscience, New York, 1992.
- 38. D. C. Rapaport, *The Art of Molecular Dynamics Simulations*, Cambridge University Press: Cambridge, 2004.

- 39. L. Li, D. Bedrov, and G. D. Smith, "Water-induced interactions between carbon nanoparticles," *J. Phys. Chem. B*, vol. 110, pp. 10509, 2006.
- 40. J. G. Kirkwood, and F. P. Buff, "The statistical mechanical theory of surface tension," *J. Chem. Phys.*, vol. 17, pp. 338, 1949.
- 41. Y. Yourdshahyan, H. K. Zhang, and A. M. Rappe, "n-alkyl thiol head-group interactions with the Au(111) surface," *Phys. Rev. B*, vol. 63, pp. 081405, 2001.
- 42. L. Z. Zhang, W. A. Goddard III, S. Y. Jiang, "Molecular simulation study of the c(4×2) superlattice structure of alkanethiol self-assembled monolayers on Au(111)," *J. Chem. Phys.*, vol. 117, pp. 7342, 2002.
- 43. M. Tachibana, K. Yoshizawa, A. Ogawa, H. Fujimoto, R. Hoffmann, "Sulfur-gold orbital interactions which determine the structure of alkanethiolate/Au(111) self-assembled monolayer systems," *J. Phys. Chem. B*, vol. 106, pp. 12727, 2002.
- 44. Y. C. Wu, J. S. Lin, S. P. Ju, W. J. Lee, Y. S. Lin, C. Hwang, "The behavior of water molecules nanoconfined between parallel Au plates," *Computational Materials Science*, vol.39, pp.359, 2007.
- 45. T. A. Sorenson, S. A. Morton, G. D. Waddill, J. A. Switzer, "Epitaxial electrodeposition of Fe3O4 thin films on the low-index planes of gold," *J. Am. Chem. Soc.*, vol.124, pp.7604, 2002.
- 46. A. A. Vertegel, M. G. Shumsky, J. A. Switzer, "Epitaxial electrodeposition of thallic oxide on single crystal

gold," Electrochimica Acta, vol.45, pp.3233, 2000.

47. S. Mullegger, S. Mitsche, P. Polt, K. Hanel, A. Birkner, C. Woll, A. Winkler, "Substrate structure dependence of the growth modes of p-quaterphenyl thin films on gold," *Thin Solid Films*, vol.484, pp.408, 2005.

Table 1 Optimized parameters used in the Dreiding force field

Interaction	D (Kcal/mol)	r(Å)	5
Au-C	0.064	3.561	12.0
Au-H	0.041	3.082	12.0
Au-O	0.048	3.395	12.0

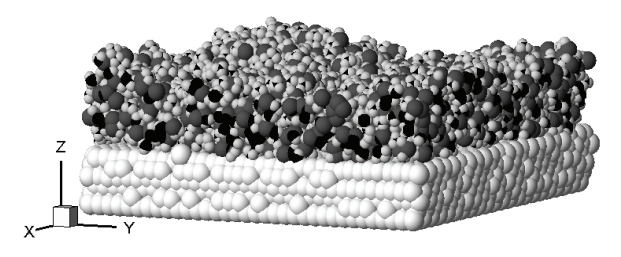


Figure 1 Relaxed model of the MMA thin film on the Au (111) substrate.

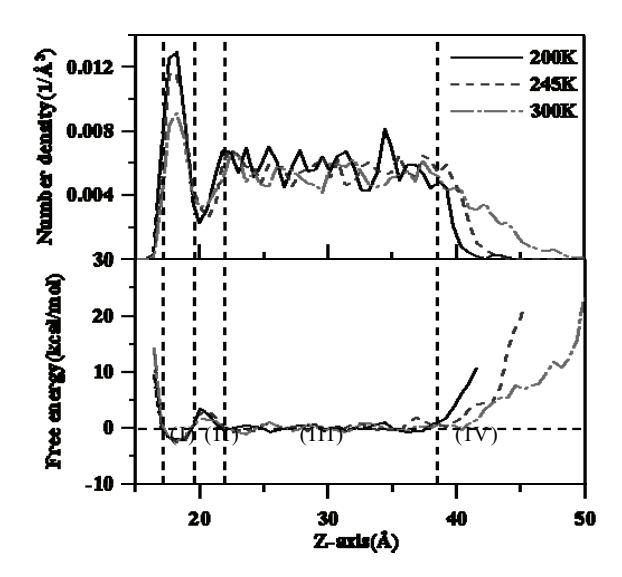


Figure 2 Variations of number density and free energy across thickness of the MMA thin film at different temperatures, where vertical dashed lines are used to indicated

the four distinct regions (I: contact, II: transition, III: bulk, IV: surface).

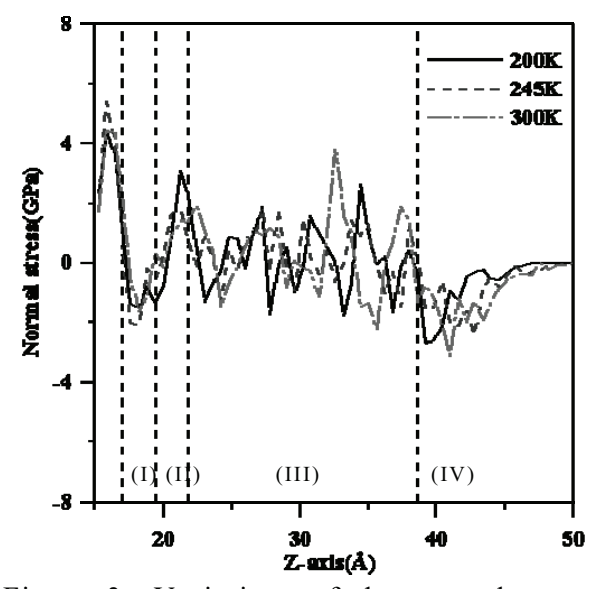


Figure 3 Variations of the normal stress across thickness of the MMA thin film at different temperatures.

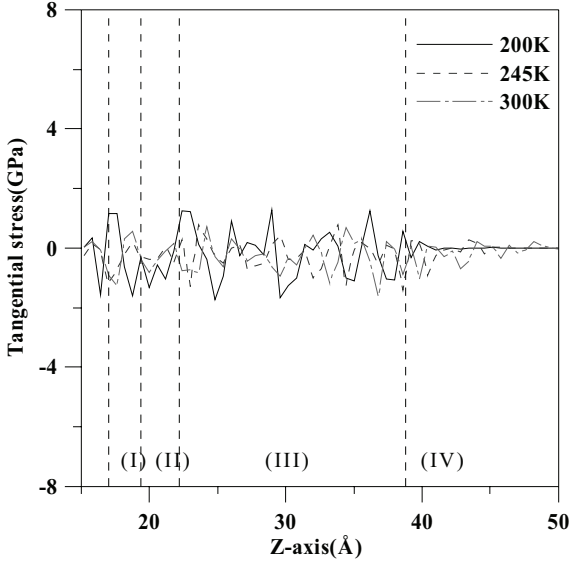


Figure 4 Variations of the tangential stress across thickness of the MMA thin film at different temperatures.

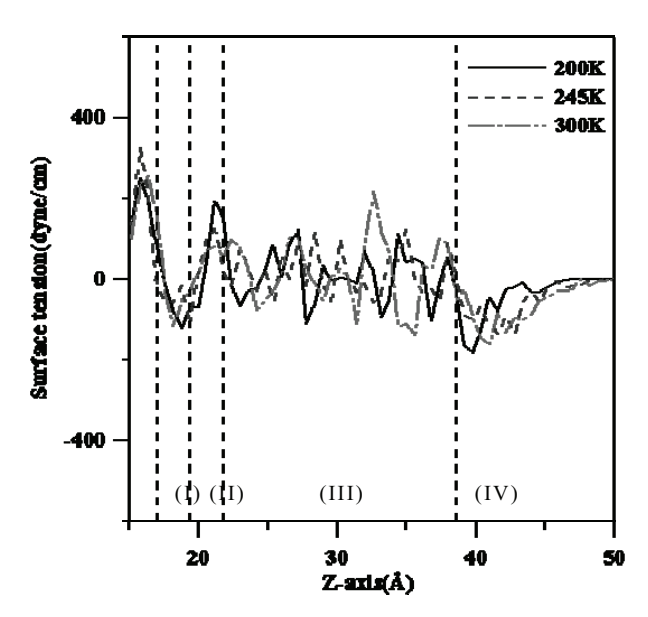


Figure 5 Variations of the surface tension across thickness of the MMA thin film at different temperatures.